Organic Electronics 92 (2021) 106137

Contents lists available at ScienceDirect

Organic Electronics

journal homepage: http://www.elsevier.com/locate/orgel

Energy levels in dilute-donor organic solar cell photocurrent generation: A thienothiophene donor molecule study

Lakshmi N.S. Murthy [a], Aaron Kramer [b], Boya Zhang [a], Jing-Mei Su [c], Yi-Sheng Chen [c], Ken-Tsung Wong [c,d,**], William G. Vandenberghe [a,***], Julia W.P. Hsu [a,*]

[a] Department of Materials Science and Engineering, University of Texas at Dallas, Richardson, TX, 75080, USA
[b] Department of Physics, University of Texas at Dallas, Richardson, TX, 75080, USA
[c] Department of Chemistry, National Taiwan University, Taipei, 10617, Taiwan
[d] Institute of Atomic and Molecular Science, Academia Sinica, Taipei, 10617, Taiwan

ARTICLE INFO

Keywords:
Dilute-donor organic solar cells
Photocurrent mechanism
Exciton dissociation
Density functional theory
Hole back transfer
Exchange-correlation functionals

ABSTRACT

To investigate photocurrent generation mechanisms in these organic solar cells (OSCs), we design and synthesize four thienothiophene (TT)-based small-molecule donors with the highest occupied molecular orbital (HOMO) levels varying from −6.4 eV to −5.1 eV, which span across the HOMO value of the [6,6]-phenyl-C70-butyric acid methyl ester ($PC_{71}BM$) acceptor. We measure TT-based donor:$PC_{71}BM$ films' electronic and optical properties, OSC current density-voltage characteristic, and external quantum efficiency, and perform density functional theory (DFT) calculations. Our results show that photocurrent generation depends strongly on the substitutions of the center TT groups, cyano (-CN) versus hexyloxy (-OHex). With 1 wt% donor, TTOHex:$PC_{71}BM$ devices produce seven times, increasing to twelve times for 5 wt % donor, higher photocurrent than neat $PC_{71}BM$ devices. In contrast, TTCN:$PC_{71}BM$ devices do not generate additional photocurrent even with 10 wt% donor. The photocurrent generation in TT-based donor:$PC_{71}BM$ devices depends critically on the HOMO value of the donor molecule with respect to that of $PC_{71}BM$, indicating the importance of type II energy level alignment to facilitate exciton dissociation at the donor-acceptor interface. The photovoltage of all TT:$PC_{71}BM$ devices are comparable to neat $PC_{71}BM$ devices, 0.85–0.90 V, with a low voltage loss due to non-radiative recombination. The fill factor of TTOHex:$PC_{71}BM$ devices are low due to the low hole mobility, $\sim 10^{-8}$ cm^2/V. Following exciton dissociation, hole transport is analyzed according to three possible mechanisms: tunneling, percolation pathways, and hole back transfer. We find that the hole back transfer mechanism can explain all experimental results and therefore is the primary hole transport mechanism for photocurrent generation in TT-based donor:$PC_{71}BM$ dilute-donor OSCs.

1. Introduction

Dilute-donor organic solar cells (OSCs), with a minute amount of donor molecules in the active layer, are intriguing because they exhibit high open-circuit voltage (V_{oc}) and short circuit current density (J_{sc}) concurrently [1–9]. The high V_{oc} is attributed to reduced bimolecular recombination [3] or the formation of a Schottky barrier between the fullerene matrix and the anode [1,2,10]. Dilute-donor OSCs have predominant exciton generation on the acceptors, followed by the formation of charge-transfer (CT) states at donor-acceptor interfaces, which can dissociate into electron-hole pairs [11]. However, the realization of J_{sc} in these solar cells remains under debate.

Conventional understanding of bulk heterojunction (BHJ) OSCs would lead to a conclusion that dilute-donor OSCs should not produce much photocurrent because there are too few donors to form a percolating pathway to the anode, thus impeding hole transport. Electron transport is not impeded as the acceptor matrix readily provide pathways to the cathode. Experimental observations however do show significant J_{sc}, which has given rise to three proposed hole transport mechanisms. First, Melianas et al. reported that hole transport in 4–7 wt

* Corresponding author.
** Corresponding author. Department of Chemistry, National Taiwan University, Taipei, 10617, Taiwan.
*** Corresponding author.
E-mail addresses: kenwong@ntu.edu.tw (K.-T. Wong), william.vandenberghe@utdallas.edu (W.G. Vandenberghe), jwhsu@utdallas.edu (J.W.P. Hsu).

https://doi.org/10.1016/j.orgel.2021.106137
Received 1 November 2020; Received in revised form 2 March 2021; Accepted 2 March 2021
Available online 8 March 2021

% dilute-donor devices are governed by donor-donor tunneling distances up to 4 nm [12]. Second, many groups proposed that for ≥10 mol % donor concentration, donor aggregation could form percolating pathways to the anode for hole transport [5,6,13]. Third, Albes et al. reported that hole transport to the anode is carried by the fullerene matrix. Following exciton dissociation and hole transferred to the donors, because of the lack of percolation pathways, holes pile up at donor sites; the resulting Coulombic repulsion drives the holes back onto fullerene molecules overcoming the donor-acceptor highest occupied molecular orbital (HOMO) energy barrier, hence "hole back transfer", and subsequently holes are transported to the anode [7]. To distinguish among these three proposed processes, combined experimental and modeling efforts are needed. For solution-processed dilute-donor OSCs, previous work all used polymer donors [2,14]. Since each polymer chain has different molecular weights and shapes, even when isolated, it is challenging to perform modeling in these polymer donor systems. An investigation of dilute-donor OSCs using small molecule dilute-donors offers more realistic modeling to gain better understanding because each molecule is small and has an identical molecular weight and shape.

In our work, we study the photocurrent in [6,6]-phenyl-C70-butyric acid methyl ester ($PC_{71}BM$)-based devices with thienothiophene (TT)-based small-molecule donors with concentrations varying from 0 to 10 wt%. The experimental investigation is complemented by planewave density functional theory (DFT) calculations. First, we elucidate donor molecule design from planewave DFT calculations with supercells. Second, we fabricate TT-based donor:$PC_{71}BM$ dilute-donor OSCs with varying donor concentration to study concentration effects on J_{sc} using ellipsometry, electrochemical impedance spectroscopy (EIS), transfer matrix method (TMM) calculations, and current density-voltage (J-V) characteristics. Third, we calculate frontier [HOMO, lowest unoccupied molecular orbitals (LUMO)] energy levels of TT-based donor-$PC_{71}BM$ dimers using DFT and show the donor-$PC_{71}BM$ interaction impact on device performance explicitly. Finally, to distinguish the three hole transport mechanisms (tunneling, aggregation, or back-transfer), we calculate the average donor-donor separation distance, measure the degree of TT-molecule aggregation using ultraviolet–visible (UV–Vis) absorption spectroscopy, atomic force microscopy (AFM), grazing incident X-ray diffraction (GIXRD), and determine the hole back transfer barrier height at the donor-acceptor interface from photovoltaic external quantum efficiency (EQE_{PV}), electroluminescence (EL) spectroscopy measurements. Our results establish that the hole back-transfer mechanism governs the photocurrent in these dilute-donor OSCs with small-molecule donors.

2. Results and discussion

2.1. Design of TT-based molecules

We design four acceptor-donor-acceptor (A-D-A)-configured molecules, in which the central donor TT-core unit is modified by two either electron deficient cyano (-CN) or electron rich hexyloxy (-OHex) groups that are symmetrically bridged by alkyl substituted thiophene units to either dicyanovinyl (-DC) or rhodanine (-RH) end acceptor groups. Fig. 1a shows the chemical structure of the four derived donor molecules: TTCN-DC, TTCN-RH, TTOHex-DC and TTOHex-RH. The TT-core unit, consisting of planar fused aromatic rings, is an electron-donating moiety [15,16], and has been reported to exhibit enhanced charge carrier mobility, higher J_{sc}, and better device performance compared to unfused aromatic rings in BHJ OSCs [17]. It has been reported that the conjugated system with the –CN group deepens the HOMO level [18], while the -OHex substituent elevates the HOMO levels and enhances the solubility of polymers [19]. In addition, the molecules end-capped with –RH groups have also been shown to deepen both HOMO and LUMO levels [20].

Our DFT calculations (detailed methodology given in supplementary information) of isolated molecules elucidate our molecular designs. Starting with the TT core, both end groups (-DC and –RH) and –CN group make the HOMO level deeper (-DC deepens the most while –RH deepens the least) while only the -OHex group makes the HOMO level shallower (Fig. S1). Permutation of end and center substitution groups produces four molecules with HOMO energies ranging between −6.4 eV and −5.1 eV as seen in Table 1. In Table 1, our calculated HOMO levels of TTCN-RH, TTOHex-DC, and TTOHex-RH are shallower than the HOMO of the $PC_{71}BM$, making them possible good donor candidates, while TTCN-DC has a deeper HOMO than $PC_{71}BM$ and is an unsuitable donor. To confirm HOMO level predictions, we synthesize the four molecules and perform cyclic voltammetry (CV) measurements. See supplementary information for molecule synthesis (Scheme S1, Figs. S2–S5), and characterization (Table S1, Fig. S6). In Table 1, we find excellent theoretical-experimental agreement on HOMO energy order, which from the shallowest to the deepest is TTOHex-RH, TTOHex-DC, TTCN-RH, then TTCN-DC when taking solvent interactions into account (Fig. S7). An in-depth statistical study on the solvent effect is outside the scope of this

Table 1
Energy levels of TT molecules from hybrid-DFT (HSE06) and CV measurements in dichloromethane (DCM) solutions. The hybrid-DFT uses an explicit solvent model for solvent interactions. CV results are shown in Fig. S6 and Table S1.

Molecules	Hybrid-DFT Calculation		Solution CV Measurement	
	HOMO (eV)	LUMO (eV)	HOMO (eV)	LUMO (eV)
TTCN-DC	−6.42	−4.47	−6.09	−3.72
TTCN-RH	−5.81	−3.98	−5.73	−3.52
TTOHex-DC	−5.72	−3.96	−5.42	−3.53
TTOHex-RH	−5.13	−3.47	−5.22	−3.42
$PC_{71}BM$	−5.92[a]	−3.84[a]	−5.87	−3.91

[a] Hybrid-DFT calculation on $PC_{71}BM$ monomer does not include DCM solvation effects.

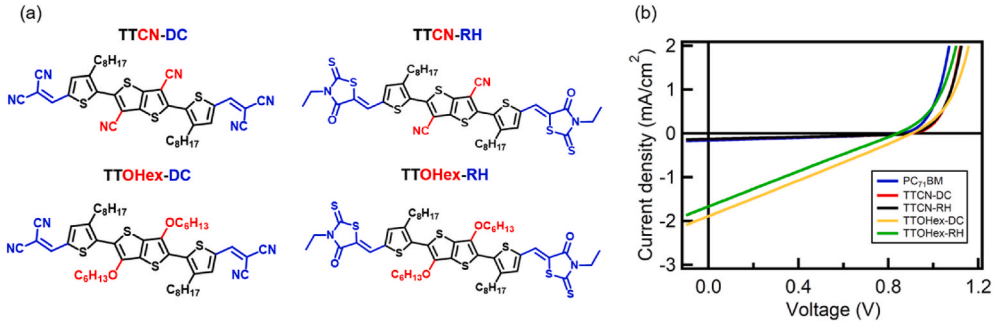

Fig. 1. (a) Molecular structures of TTCN-DC, TTCN-RH, TTOHex-DC, and TTOHex-RH. (b) J-V curves of neat $PC_{71}BM$ (blue) and 5 wt% TT-based donor:$PC_{71}BM$ devices with TTCN-DC (red), TTCN-RH (black), TTOHex-DC (yellow), and TTOHex-RH (green) donor molecules under one-sun illumination (AM 1.5G 100 mW/cm^2). (For interpretation of the references to color in this figure legend, the reader is referred to the Web version of this article.)

paper and will be the subject of a future publication [21]. In terms of absolute HOMO energy values, theoretical DFT and experimental CV agree within 0.1 eV for both the RH molecules, while theory predicts a deeper HOMO for both DC molecules by 0.3 eV. Based on theoretical HOMO values with respect to that of $PC_{71}BM$, we expect TTOHex-RH:$PC_{71}BM$ and TTCN-DC:$PC_{71}BM$ devices to generate the most and least photocurrent respectively.

After characterizing the donor molecules in solution, we fabricate the TT donor thin films and perform UV–Vis absorption spectroscopy and PESA measurements. When donor molecules condense to a solid state, the molecular interactions alter the energy levels. Compared to molecules in solution, both the absorbance peaks of TTOHex molecules in thin films red shift, i.e. smaller optical band gap (Fig. S8a). Using PESA, we determine the ionization energy (IE) of neat $PC_{71}BM$, TTCN-RH, and TTOHex films (Fig. S8b). From the IE and optical bandgap values shown in Table 2, we find that TTOHex films form a type II energy level alignment with neat $PC_{71}BM$ films, while TTCN-RH films form a type I energy level alignment with neat $PC_{71}BM$ films. In BHJ-OSCs, energy level alignment using pristine donor and pristine acceptor energy levels are used to forecast exciton dissociation and charge generation at the donor-acceptor interface. For dilute-donor OSCs, donor domains are as small as isolated molecules, possibly with significantly different properties compared to the pristine film phase. It is therefore not clear that a type II energy level alignment of pristine compounds is a necessary criterion for charge generation through CT states. This issue has not been studied previously. In this paper, we examine the role of energy level alignment in the photocurrent generation.

2.2. Photocurrent generation in TT-based donor:$PC_{71}BM$ dilute-donor OSCs

To test how the TT-based donors with different HOMO energy levels affect photocurrent generation in dilute-donor devices, we measure the J-V curves of neat $PC_{71}BM$ and four 5 wt% TT-based donor:$PC_{71}BM$ devices under AM 1.5 one-sun illumination (Fig. 1b) and in dark (Fig. S10). Device parameters obtained from Fig. 1b are shown in Table 3. TTOHex:$PC_{71}BM$ (TTOHex-DC:$PC_{71}BM$, TTOHex-RH:$PC_{71}BM$) devices generate additional photocurrent (J_{sc} ~ 1.67–1.90 mA/cm^2), which is at least 10 times larger than neat $PC_{71}BM$ (J_{sc} ~ 0.16 mA/cm^2). Strikingly, TTCN:$PC_{71}BM$ (TTCN-DC:$PC_{71}BM$, TTCN-RH:$PC_{71}BM$) devices generate the same amount of photocurrent as neat $PC_{71}BM$, i.e. no additional photocurrent generation. Despite the low leakage current in the dark J-V curves (Fig. S10), these devices show low J-V performance under illumination. But these results are highly reproducible from batch to batch. EQE_{PV} results (Fig. S11) also confirm that TTCN:$PC_{71}BM$ and neat $PC_{71}BM$ devices generate the same low EQE (maximum ~ 3%), whereas TTOHex:$PC_{71}BM$ produce substantially larger EQE (maximum 15–21%). These results indicate that the chemical nature of the center substitution groups (-CN vs -OHex) has a stronger effect on the photocurrent than the end groups (-DC vs –RH).

2.3. DFT calculations of HOMO energies of TT-$PC_{71}BM$ dimers

To understand how interactions between TT-based molecules and $PC_{71}BM$ affect energy level positions, we perform DFT calculations of TT-$PC_{71}BM$ dimers in large supercells (detailed supercell methodology given in supplementary information). Supercells, as opposed to unit cells, are more appropriate for planewave DFT calculations on lower dimensional materials or molecules [22–24]. Fig. 2 shows HOMO-LUMO energy levels of interacting TT-$PC_{71}BM$ dimers compared to a $PC_{71}BM$-$PC_{71}BM$ dimer, as well as frontier orbital localization of all dimers. Interaction with $PC_{71}BM$ makes the HOMO levels shallower for TT-based molecules with -DC end groups and has negligible effects on TT-based molecules with –RH end groups for all dimer configurations we studied (Fig. S9). $PC_{71}BM$ interaction with another $PC_{71}BM$ molecule shallows the HOMO for the $PC_{71}BM$-$PC_{71}BM$ dimer and has delocalized charges on both molecules. The HOMO energy of TTCN-DC-$PC_{71}BM$ dimer is 0.32 eV deeper than $PC_{71}BM$-$PC_{71}BM$ dimer's HOMO level, and HOMO localization is observed on the $PC_{71}BM$ instead of the TTCN-DC as seen in Fig. 2b. Therefore, in TTCN-DC:$PC_{71}BM$ devices, exciton dissociation will not be favorable. It is consistent with the experiments in Fig. 1b where we observe the same photocurrent for TTCN-DC:$PC_{71}BM$ and neat $PC_{71}BM$ devices.

Fig. 2a also shows that dimers of TTOHex-DC and TTOHex-RH with $PC_{71}BM$ respectively have 0.22 eV and 0.72 eV shallower HOMO energies than the $PC_{71}BM$-$PC_{71}BM$ dimer's HOMO energy. From Fig. 2b, we then observe HOMO localizations on the TT-based molecules. Thus, both TTOHex:$PC_{71}BM$ devices have an energy level alignment strongly favoring exciton dissociation. Measurements of neat TTOHex films show shallower IE levels than $PC_{71}BM$ (Table 2, Fig. S8b), agreeing with the DFT results. Accordingly, in Fig. 1b, we observe a 10x higher J_{sc} compared to neat $PC_{71}BM$ for both TTOHex:$PC_{71}BM$ devices at 5 wt% donor concentration.

That the HOMO of TTCN-RH-$PC_{71}BM$ is slightly shallower (0.10 eV) than that of the $PC_{71}BM$-$PC_{71}BM$ dimer and HOMO is localized on the TTCN-RH molecule, as Fig. 2 shows, indicating that exciton dissociation is possible in TTCN-RH:$PC_{71}BM$ devices on theoretical grounds, albeit less favored compared to TTOHex:$PC_{71}BM$ devices. Experimentally, however, we do not observe any J_{sc} increase (Fig. 1b). IE measurement of the TTCN-RH film exhibits a deeper IE than $PC_{71}BM$ (Table 2, Fig. S8b). Thus, no significant exciton dissociation can be realized. We attribute the discrepancy between theory and experiment to additional intermolecular interactions which we cannot account for in the simulations due to computational limitations.

Our experiments and theoretical results explain that TTCN-$PC_{71}BM$ interface has unfavorable film IE values (Table 2) and HOMO localizations (Fig. 2b) on donor and acceptor, thus prevents exciton dissociation. In contrast, TTOHex-$PC_{71}BM$ interface has suitable film IE values and HOMO localizations to facilitate exciton dissociation. While some non-fullerene acceptor based OSCs suggest energy offsets at the D/A heterojunction is not required for exciton dissociation [25], these results show that energy offset between donor and acceptor is critical for exciton dissociation, thus photocurrent generation, in these dilute-donor OSCs.

2.4. Effect of donor concentration on photocurrent generation

Next, we investigate the donor concentration dependence on the photocurrent generation, we fabricate and measure the J-V curves in TT-

Table 2
Ionization energy (IE) of $PC_{71}BM$, TTCN-RH, TTOHex-DC, TTOHex-RH films obtained from photoelectron spectroscopy in air (PESA) (Fig. S8b) and optical bandgap from UV–Vis spectra (Fig. S8a).

Samples	IE (eV)	Optical bandgap (eV)
$PC_{71}BM$	−5.85	1.75
TTCN-RH	−5.92	1.91
TTOHex-DC	−5.36	1.77
TTOHex-RH	−5.35	1.74

Table 3
Device parameters of neat $PC_{71}BM$ and 5 wt% TT-based donor:$PC_{71}BM$ devices with TTCN-DC, TTCN-RH, TTOHex-DC, and TTOHex-RH donor molecules. The standard deviations are calculated from at least 10 diodes from different runs.

Samples	V_{oc} (mV)	J_{sc} (mA/cm^2)	FF	PCE (%)
$PC_{71}BM$	855 ± 12	0.16 ± 0.01	0.32 ± 0.01	0.04 ± 0.00
TTCN-DC	891 ± 8	0.13 ± 0.00	0.32 ± 0.01	0.04 ± 0.00
TTCN-RH	909 ± 8	0.13 ± 0.00	0.31 ± 0.00	0.04 ± 0.00
TTOHex-DC	902 ± 11	1.90 ± 0.06	0.26 ± 0.00	0.44 ± 0.02
TTOHex-RH	844 ± 7	1.67 ± 0.06	0.25 ± 0.00	0.35 ± 0.01

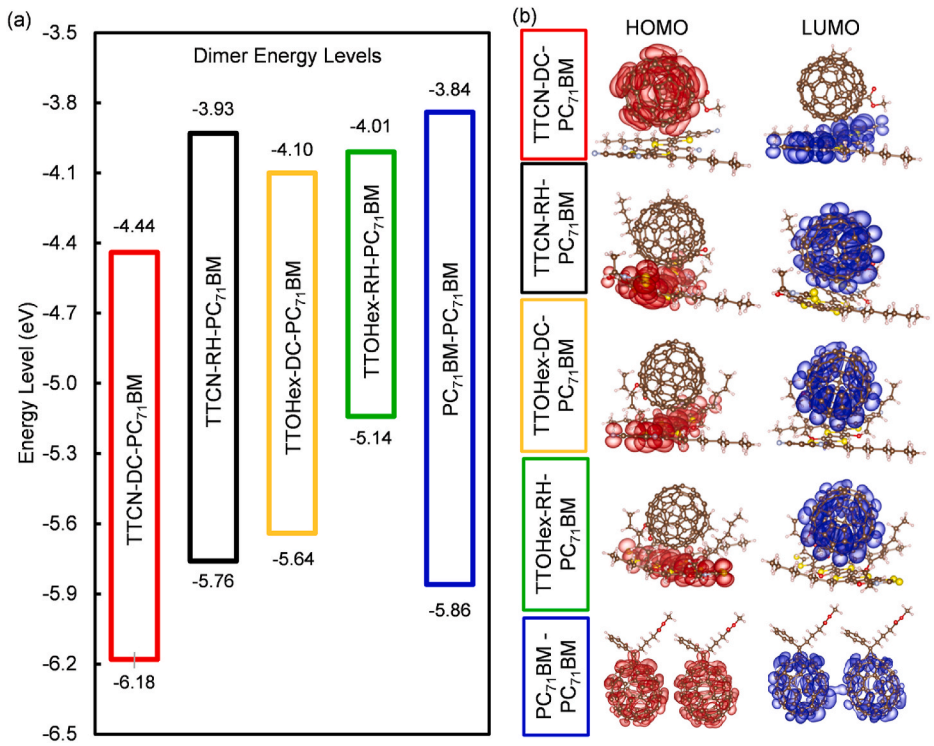

Fig. 2. (a) Comparison of the HOMO-LUMO energy levels of four TT-$PC_{71}BM$ dimers and a $PC_{71}BM$-$PC_{71}BM$ dimer. (b) The frontier orbital localizations of TT-$PC_{71}BM$ dimers and the $PC_{71}BM$-$PC_{71}BM$ dimer.

based donor:$PC_{71}BM$ devices with three donors: TTOHex-DC (Fig. 3a), TTCN-DC (Fig. S12a), and TTOHex-RH (Fig. S12b) with concentrations varying from 0 to 10 wt%. To confirm the donor concentration (wt.%) in TTOHex-DC:$PC_{71}BM$ films, we quantify the sulfur (S) concentration (S/(C + O + S) at.%) from energy-dispersive X-ray spectroscopy (EDX). Sulfur is used as a proxy for the TTOHex-DC donors because $PC_{71}BM$ does not contain S. Fig. S13 shows the average S at.% increases with the TTOHex-DC wt.% and is consistent with calculated S at.% in the TTOHex-DC:$PC_{71}BM$ films based on nominal donor concentrations (Table S2), confirming increasing donor concentrations in the blends.

Device parameters of these devices are shown in Table S3. $PC_{71}BM$ devices with both TTOHex donors exhibit similar monotonic J_{sc} increase as a function of donor concentration while TTCN-DC:$PC_{71}BM$ devices do not generate additional photocurrent even at 10 wt% concentration

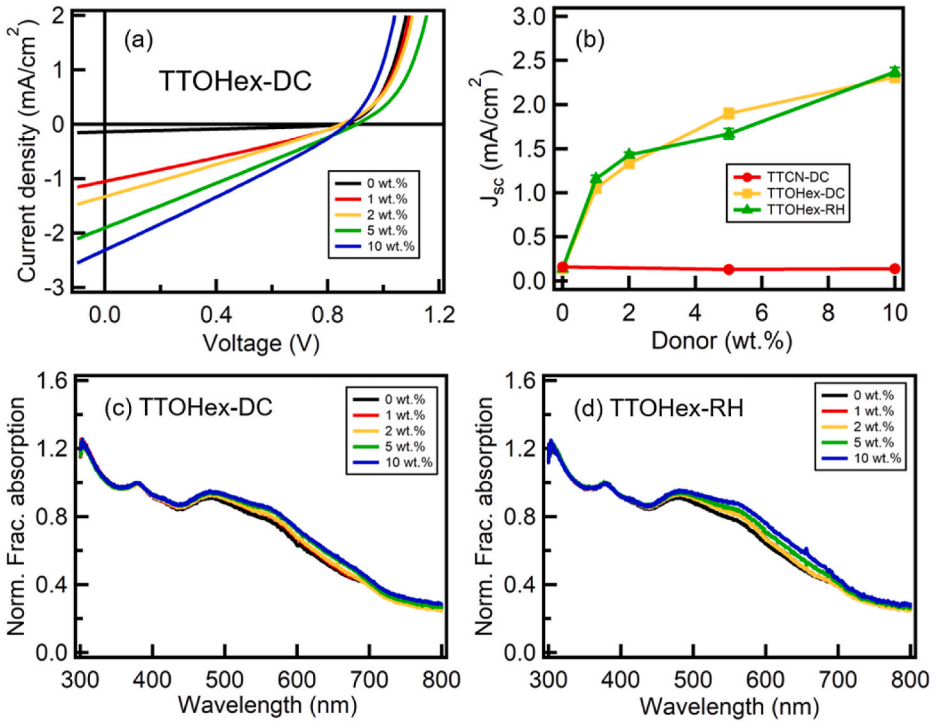

Fig. 3. (a) J-V curves of TTOHex-DC:$PC_{71}BM$ devices with different donor concentrations: 0 wt% (black), 1 wt% (red), 2 wt% (yellow), 5 wt% (green), and 10 wt% (blue) under illumination (AM 1.5G 100 mW/cm^2). (b) J_{sc} vs donor wt.% in TT-based donor:$PC_{71}BM$ devices for TTCN-DC (closed red circles), TTOHex-DC (closed yellow squares), and TTOHex-RH (closed green triangles) molecules. These results are averaged over at least 5 devices for each type. Fractional absorption spectra normalized at 380 nm of TTOHex:$PC_{71}BM$ for (c) TTOHex-DC and (d) TTOHex-RH molecules with different donor concentrations: 0–10 wt%. The color schemes used in (c) and (d) are the same as in (a). (For interpretation of the references to color in this figure legend, the reader is referred to the Web version of this article.)

(Fig. 3b). In TTOHex:$PC_{71}BM$ devices, 1 wt% TTOHex donors J_{sc} increases about 7-fold, from ~0.14 to ~1.1 mA/cm^2. With the further addition of TTOHex donors from 1 to 10 wt%, J_{sc} increases much less dramatically, only by about a factor of 2. Fig. 3c,d shows the normalized fractional absorption spectra in the donor absorption region (500–700 nm from Fig. S8a) increases with the donor concentration. To study the effect of donor absorption on J_{sc}, we perform Transfer Matrix Method (TMM) [26,27] calculations on TTOHex-RH:$PC_{71}BM$ devices using complex optical constants determined from ellipsometry for the different donor concentration absorber layers. Because TMM assumes 100% internal quantum efficiency (IQE), to compare with experiments, the J_{sc} of the neat $PC_{71}BM$ device is subtracted from J_{sc} of the dilute donor devices (Fig. S14). The results show that J_{sc} from TMM and experiments behave similarly, indicating that the J_{sc} increase with the donor concentration results from the contribution of donor absorption. Note that V_{oc} is independent of donor concentration and remains above 0.83 V, which can be attributed to the low non-radiative voltage losses (ΔV_{NR}). For 5 wt% TTOHex-RH:$PC_{71}BM$ devices, EQE_{EL} of 2.67×10^{-5} (taken at a bias with injected current equal to J_{sc}) translates to ΔV_{NR} of 270 ± 4 mV (average over 5 diodes) using $\Delta V_{NR} = \frac{kT}{q} \ln \frac{1}{EQE_{EL}}$ [28]. Low fill factor (FF) of ~0.2–0.3 is observed in all TT:$PC_{71}BM$ devices and independent of donor concentration, which indicates poor charge extraction in these devices. We measure charge carrier mobilities by fabricating hole-only devices of 0, 1, 2, 5 wt% TTOHex-DC:$PC_{71}BM$ and extracting hole mobility using the space charge limited current (SCLC) model (Table S4). All hole mobilities are in the range of $1–3 \times 10^{-8}$ $cm^2V^{-1}s^{-1}$ and independent of donor concentration. The consistency of these SCLC hole mobilities values are confirmed by measuring active layers with different thicknesses (Fig. S15). These low hole mobilities are the main reason for the low FF in these devices. Additionally, FF can be reduced by enhanced recombination. To study the recombination characteristics, we perform EIS at open circuit condition under white-light illumination at 100 mW/cm^2. Fig. S16 shows that 5 wt% TTOHex:$PC_{71}BM$ devices have lower recombination resistances, i.e., enhanced recombination, than 5 wt% TTCN:$PC_{71}BM$ devices (Table S5). These results are consistent with that TTOHex:$PC_{71}BM$ devices exhibit lower FF than TTCN:$PC_{71}BM$ devices.

Previous research showed that dilute-donor OSCs with other donors also show similar J_{sc} dependence on donor concentration [4,14,29]: J_{sc} rises significantly with 1–2 wt% donor addition, followed by a gradual increase at higher donor concentrations. The saturation of J_{sc} with increasing donor content results from competing photocurrent loss mechanisms between exciton dissociation and nongeminate recombination [4]. Therefore, it is important to understand the mechanism by which photocurrent is generated in 1 wt% TTOHex:$PC_{71}BM$ devices, where donor molecules are mostly isolated in the $PC_{71}BM$ matrix and are unlikely to form a percolation path for hole transport.

2.5. Hole transport mechanisms

Even after excitons are successfully dissociated at the donor-acceptor interface, the question remains on how holes transport to the anode with discontinuous donor domains. Here, we consider three proposed hole transport mechanisms—tunneling [12], percolating pathways [5,6,13], and hole back transfer [7]— for our molecular systems.

2.5.1. Tunneling between isolated donor molecules

To estimate the tunneling distance, we use the mass density of $PC_{71}BM$ and calculate the molecule volume of TTOHex-DC and TTOHex-RH molecules using DFT. Since TTOHex densities are not experimentally available, we relax the DFT unit cells in a periodic structure without vacuum. The final volume of the unit cell after relaxation is used as the volume of TTOHex. We find that the average distance between two TTOHex molecules is ≥ 4.6 nm at 1 wt% (Table S6). Tunneling probability for holes over such a distance is completely negligible. Melenias et al. experimentally observe photocurrent in 1.5 mol% donor devices that have an average donor-donor distance of 5.35 nm which is larger than our TTOHex-TTOHex distances [12]. Melianas et al. attribute their current to tunneling using $m^* = 0.032m_e$ and kinetic energy of 0.75 eV when fitting with a Fowler-Nordheim model. If such kinetic energy and effective mass were realized in our devices, tunneling would have also been possible. However, such a small effective mass has never been observed in organic systems and it is unclear what the source of a 0.75 eV kinetic energy would be. Hence tunneling between isolated donor molecules probably does not contribute much to hole transport in these devices.

2.5.2. Percolation arising from donor aggregation

The hole transport in the dilute donor devices can also occur by percolating pathways that are formed by donor molecules aggregating together instead of dispersing through the fullerene matrix. The UV–vis absorption spectra of TTOHex:$PC_{71}BM$ films (Fig. 3c,d) show absorption increases in the donor absorption region (500–700 nm from Fig. S8a) with increasing donor concentration. These results indicate that both TTOHex molecules contribute to the dilute donor film absorption. But it does not indicate the presence of donor aggregation in these films.

To directly probe whether the aggregation of donor molecules exists in the active layer, we perform AFM and GIXRD measurements on 10 wt % TTOHex-RH:$PC_{71}BM$ films. AFM topographic images (Fig. 4a) shows a uniform surface texture without obvious crystalline regions and the root mean square (RMS) roughness is small ~ 1 nm, which is consistent with the amorphous nature indicated in the GIXRD results. Fig. 4b shows the GIXRD patterns of neat TTOHex-RH and 10 wt% TTOHex-RH:$PC_{71}BM$ films [30]. We observe a strong peak at ~6° for the neat TTOHex-RH film, whereas the 10 wt% TTOHex-RH film does not show any peak. These results provide evidence that there is little or no donor aggregation in the active layer.

In a modeling study, Hussian et al. showed that J_{sc} increases only when the aggregation pathways reach the hole-collecting electrodes [31]. Experimentally the J_{sc} increase from 2 to 5 wt% donor (Fig. 3b) is not substantial, indicating that even if aggregation exists, it contributes little to photocurrent generation. We further vary the device architecture to confirm this conclusion. Since forming percolating paths to anode depends on donor interaction with the hole transport layer material. The J-V curves in the inverted 5 wt% TTOHex:$PC_{71}BM$ devices (Fig. S17, Table S7) also generate photocurrent, albeit less. Since the anode is MoO_3 on top of the active layer in the inverted structure versus poly (3,4-ethylenedioxythiophene):poly (styrenesulfonate) (PEDOT:PSS) below the active layer in the conventional architecture, it is unlikely that the percolation paths reach the anode in both device architectures. Hence, percolating pathways cannot be considered as a hole transport mechanism.

2.5.3. Hole back transfer from donor molecules to $PC_{71}BM$ matrix

In the hole back transfer mechanism, exciton dissociation results in holes on the donor molecules and electrons on the $PC_{71}BM$ matrix. For holes to be able to transport to the anode, they must overcome the barrier at the donor-acceptor interface and transfer back to the $PC_{71}BM$ matrix, the only continuous component in the active layer. Albes et al. calculated that the barrier height must be ≤ 0.4 eV; since this barrier comes from an energy offset (ΔE), it can be determined by $\Delta E = E_g$ (acceptor) - E_{CT}, where E_{CT} is the charge transfer (CT) state energy and E_g (acceptor) is the optical band gap of the acceptor [7]. To measure this barrier height, we perform low-energy EQE_{PV} spectroscopy. Fig. 5 shows that the EQE_{PV} signal decreases exponentially at the $PC_{71}BM$ band gap (1.75 eV) for the neat $PC_{71}BM$ device, while all TTOHex:$PC_{71}BM$ devices exhibit EQE_{PV} signals below this energy. By fitting this low-energy EQE_{PV} tail with a Gaussian curve, the charge transfer state energy (E_{CT}) and reorganizational energy (λ) are extracted [32]. We find that E_{CT} is independent of donor concentration: 1.73 eV for TTOHex-DC:$PC_{71}BM$ and 1.72 eV for TTOHex-RH:$PC_{71}BM$, while λ increases with

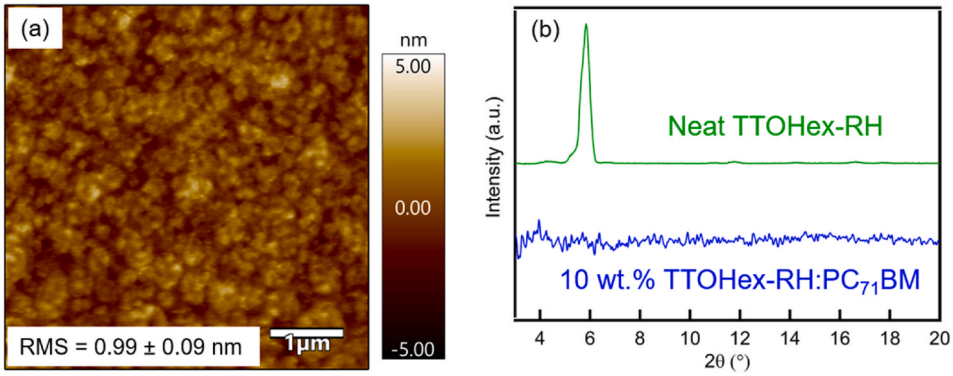

Fig. 4. (a) AFM height images of 10 wt% TTOHex-RH:$PC_{71}BM$ film. The RMS roughness values were calculated from 5 μm × 5 μm height images. (b) GIXRD patterns of neat TTOHex-RH (green) and 10 wt% TTOHex-RH:$PC_{71}BM$ (blue) films. (For interpretation of the references to color in this figure legend, the reader is referred to the Web version of this article.)

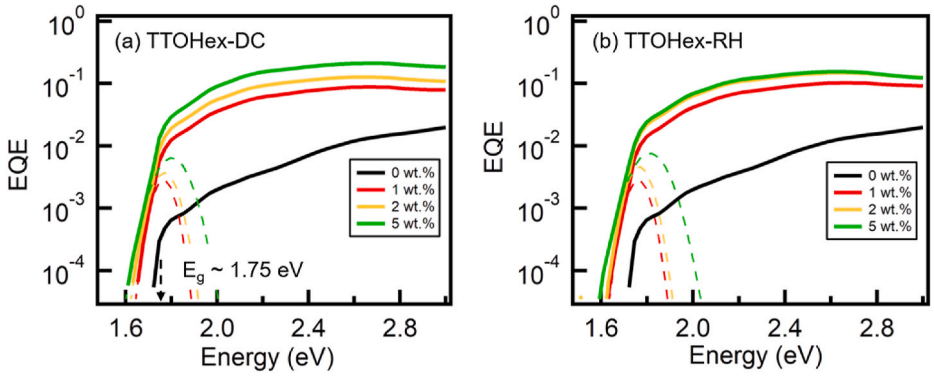

Fig. 5. EQE_{PV} (log) vs energy (solid lines) of (a) TTOHex-DC:$PC_{71}BM$ and (b) TTOHex-RH:$PC_{71}BM$ devices with different donor concentrations: 0 wt% (black), 1 wt% (red), 2 wt% (yellow), and 5 wt% (green). The dashed lines show the Gaussian fits for CT state absorption. The black dashed arrow in (a) marks the $PC_{71}BM$ band gap (E_g = 1.75 eV). (For interpretation of the references to color in this figure legend, the reader is referred to the Web version of this article.)

donor concentration but is less than 0.1 eV for all devices (Table 4). The area under the Gaussian curve, which reflects the donor-acceptor interfacial area [3], increases linearly with donor concentration for both TTOHex:$PC_{71}BM$ devices (Fig. S18), further confirming that aggregation is minor in these blends. Since Fig. 5 does not show prominent CT state shoulders in EQE_{PV} spectra, to confirm the determination of E_{CT}, we perform EL measurements on the 5 wt% TTOHex:$PC_{71}BM$ devices (Fig. S19). Similar to EQE_{PV}, fitting the EL spectra tail with a Gaussian curve yields the E_{CT} and λ [32]. From the intersection of the Gaussian fit from the EQE_{PV} and EL spectra [33], we obtain E_{CT} of 1.74 (1.76) eV for the 5 wt% TTOHex-DC (TTOHex-RH):$PC_{71}BM$ devices (Fig. S19), which are within experimental uncertainty with the value obtained from the EQE_{PV} spectrum alone. Therefore, TTOHex donors exhibit negligible ΔE, hence no barriers for holes to transfer from the donor back to the acceptor and transport through the $PC_{71}BM$ matrix to generate photocurrent. This co-existence of negligible ΔE offset and low ΔV_{NR} in our devices is consistent with the published literature [34]. Thus, hole back transfer is the primary hole transport mechanism in TT-based donor:$PC_{71}BM$ devices.

Table 4
CT state energy (E_{CT}) and reorganizational energy (λ) of 1, 2, 5 wt% TTOHex:$PC_{71}BM$ devices obtained from the Gaussian fit in the low energy EQE_{PV} (Fig. 5). ΔE was calculated using $\Delta E = E_g$ (acceptor) - E_{CT} [7].

Donor wt.%	TTOHex-DC:$PC_{71}BM$		TTOHex-RH:$PC_{71}BM$	
	E_{CT} (eV)	λ (eV)	E_{CT} (eV)	λ (eV)
1	1.73 ± 0.01	0.03 ± 0.01	1.72 ± 0.01	0.03 ± 0.01
2	1.73 ± 0.01	0.04 ± 0.01	1.72 ± 0.01	0.04 ± 0.01
5	1.73 ± 0.02	0.07 ± 0.01	1.72 ± 0.02	0.09 ± 0.03

3. Conclusions

In conclusion, we design and synthesize four TT-based small-molecule donors with different HOMO levels to probe photocurrent generation in dilute-donor OSCs. We show that photocurrent in TT-based donor:$PC_{71}BM$ devices predominantly depends on the center substitution groups (-CN vs -OHex), rather than the end groups (-DC vs –RH). A drastic increase (~7 times) of photocurrent is observed in TTOHex:$PC_{71}BM$ devices with the addition of a small amount (1 wt%) of donor molecules. In contrast, TTCN:$PC_{71}BM$ devices do not generate additional photocurrent even when introducing 10 wt% of donor molecules. Analyzing the HOMO energy levels, we show that the difference between photocurrent in TTOHex:$PC_{71}BM$ and TTCN:$PC_{71}BM$ is determined by whether excitons can dissociate at the donor-acceptor interface. The experimental results are supported by DFT calculations. We find that following exciton dissociation, hole back transfer is the mechanism responsible for photocurrent generation in these dilute-donor OSCs.

Declaration of competing interest

The authors declare that they have no known competing financial interests or personal relationships that could have appeared to influence the work reported in this paper.

Acknowledgements

We would like to thank A. Mishra and J. Slinker for performing the EL measurements, R. Wallace for the usage of the ellipsometer. This project is supported by National Science Foundation CBET-1916612 and Ministry of Science and Technology Taiwan (MOST 107-2113-M-002-019-MY3). A.K., W.G.V., and J.W.P.H. acknowledge the Texas Advanced Computing Center (TACC) at the University of Texas at Austin for providing the high-performance computing resources that have contributed to the research results provided within the paper. J.W.P.H acknowledges the Texas Instruments Distinguished Chair in Nanoelectronics.

Appendix A. Supplementary data

Supplementary data to this article can be found online at https://doi.org/10.1016/j.orgel.2021.106137.

References

[1] M. Zhang, H. Wang, H. Tian, Y. Geng, C.W. Tang, Bulk heterojunction photovoltaic cells with low donor concentration, Adv. Mater. 23 (2011) 4960–4964, https://doi.org/10.1002/adma.201102173.

[2] B. Yang, F. Guo, Y. Yuan, Z. Xiao, Y. Lu, Q. Dong, J. Huang, Solution-processed fullerene-based organic Schottky junction devices for large-open-circuit-voltage organic solar cells, Adv. Mater. 25 (2013) 572–577, https://doi.org/10.1002/adma.201203080.

[3] K. Vandewal, J. Widmer, T. Heumueller, C.J. Brabec, M.D. McGehee, K. Leo, M. Riede, A. Salleo, Increased open-circuit voltage of organic solar cells by reduced donor-acceptor interface area, Adv. Mater. 26 (2014) 3839–3843, https://doi.org/10.1002/adma.201400114.

[4] L. Xu, J. Wang, M. de A. Villa, T.B. Daunis, Y.-J. Lee, A. V Malko, J.W.P. Hsu, Quantitative analyses of competing photocurrent generation mechanisms in fullerene-based organic photovoltaics, J. Phys. Chem. C 120 (2016) 16470–16477, https://doi.org/10.1021/acs.jpcc.6b05044.

[5] J.-W. Seo, J.H. Kim, M. Kim, S.-M. Jin, S.-H. Lee, C. Cho, E. Lee, S. Yoo, J.Y. Park, J.-Y. Lee, Columnar-structured low-concentration donor molecules in bulk heterojunction organic solar cells, ACS Omega 3 (2018) 929–936, https://doi.org/10.1021/acsomega.7b01652.

[6] K. Ding, X. Liu, S.R. Forrest, Charge transfer and collection in dilute organic donor–acceptor heterojunction blends, Nano Lett. 18 (2018) 3180–3184, https://doi.org/10.1021/acs.nanolett.8b00851.

[7] T. Albes, L. Xu, J. Wang, J.W.P. Hsu, A. Gagliardi, Origin of photocurrent in fullerene-based solar cells, J. Phys. Chem. C 122 (2018) 15140–15148, https://doi.org/10.1021/acs.jpcc.8b03941.

[8] W. Jiang, C. Tao, M. Stolterfoht, H. Jin, M. Stephen, Q. Lin, R.C.R. Nagiri, P. L. Burn, I.R. Gentle, Hole-transporting materials for low donor content organic solar cells: charge transport and device performance, Org. Electron. 76 (2020) 105480, https://doi.org/10.1016/j.orgel.2019.105480.

[9] L.N.S. Murthy, B. Zhang, J.W.P. Hsu, Device architecture study in fullerene-based organic photovoltaics, J. Phys. Chem. C 124 (2020) 12982–12989, https://doi.org/10.1021/acs.jpcc.0c02956.

[10] S. Sutty, G. Williams, H. Aziz, Fullerene-based Schottky-junction organic solar cells: a brief review, J. Photon. Energy 4 (2014), 040999, https://doi.org/10.1117/1.JPE.4.040999.

[11] Y. Song, A. Schubert, X. Liu, S. Bhandari, S.R. Forrest, B.D. Dunietz, E. Geva, J. P. Ogilvie, Efficient charge generation via hole transfer in dilute organic donor–fullerene blends, J. Phys. Chem. Lett. 11 (2020) 2203–2210, https://doi.org/10.1021/acs.jpclett.0c00058.

[12] A. Melianas, V. Pranculis, D. Spoltore, J. Benduhn, O. Inganäs, V. Gulbinas, K. Vandewal, M. Kemerink, Charge transport in pure and mixed phases in organic solar cells, Adv. Energy Mater. 7 (2017) 1700888, https://doi.org/10.1002/aenm.201700888.

[13] T. Lee, A. Sanzogni, N. Zhangzhou, P.L. Burn, A.E. Mark, Morphology of a bulk heterojunction photovoltaic cell with low donor concentration, ACS Appl. Mater. Interfaces 10 (2018) 32413–32419, https://doi.org/10.1021/acsami.8b10321.

[14] B. Yang, Z. Xiao, J. Huang, Polymer aggregation correlated transition from Schottky-junction to bulk heterojunction organic solar cells, Appl. Phys. Lett. 104 (2014) 143304, https://doi.org/10.1063/1.4871306.

[15] X. Cheng, M. Li, Z. Guo, J. Yu, G. Lu, L. Bu, L. Ye, H. Ade, Y. Chen, Y. Geng, "Twisted" conjugated molecules as donor materials for efficient all-small-molecule organic solar cells processed with tetrahydrofuran, J. Mater. Chem. A. 7 (2019) 23008–23018, https://doi.org/10.1039/C9TA07760J.

[16] W. Li, Y. Guo, J. Shi, H. Yu, H. Meng, Solution-processable neutral green electrochromic polymer containing thieno[3,2- b]thiophene derivative as unconventional donor units, Macromolecules 49 (2016) 7211–7219, https://doi.org/10.1021/acs.macromol.6b01624.

[17] Y.S. Choi, W.H. Jo, A strategy to enhance both VOC and JSC of A–D–A type small molecules based on diketopyrrolopyrrole for high efficient organic solar cells, Org. Electron. 14 (2013) 1621–1628, https://doi.org/10.1016/j.orgel.2013.03.031.

[18] M.S. Liu, X. Jiang, S. Liu, P. Herguth, A.K.Y. Jen, Effect of cyano substituents on electron affinity and electron-transporting properties of conjugated polymers, Macromolecules 35 (2002) 3532–3538, https://doi.org/10.1021/ma011790f.

[19] J.A. Mikroyannidis, M.M. Stylianakis, K.Y. Cheung, M.K. Fung, A.B. Djurišić, Alternating phenylenevinylene and thienylenevinylene copolymers with cyano groups: synthesis, photophysics and photovoltaics, Synth. Met. 159 (2009) 142–147, https://doi.org/10.1016/j.synthmet.2008.08.008.

[20] J. Wang, K. Shi, Y. Suo, Y. Lin, G. Yu, X. Zhan, Monodisperse macromolecules based on benzodithiophene and diketopyrrolopyrrole with strong NIR absorption and high mobility, J. Mater. Chem. C. 4 (2016) 3781–3791, https://doi.org/10.1039/C5TC03589A.

[21] A. Kramer, J. W. P. Hsu, W. G. Vandenberghe, Explicit Solvent Effects on Thienothiophene Molecules Using First Principle Calculations, preprint.

[22] C. Song, Q. Ge, L. Wang, DFT studies of Pt/Au bimetallic clusters and their interactions with the CO molecule, J. Phys. Chem. B 109 (2005) 22341–22350, https://doi.org/10.1021/jp0546709.

[23] V.L. Deringer, J. George, R. Dronskowski, U. Englert, Plane-wave density functional theory meets molecular crystals: thermal ellipsoids and intermolecular interactions, Acc. Chem. Res. 50 (2017) 1231–1239, https://doi.org/10.1021/acs.accounts.7b00067.

[24] A. Kramer, M.L. Van de Put, C.L. Hinkle, W.G. Vandenberghe, Tellurium as a successor of silicon for extremely scaled nanowires: a first-principles study, Npj 2D Mater, Apple 4 (2020) 10, https://doi.org/10.1038/s41699-020-0143-1.

[25] L. Perdigón-Toro, H. Zhang, A. Markina, J. Yuan, S.M. Hosseini, C.M. Wolff, G. Zuo, M. Stolterfoht, Y. Zou, F. Gao, D. Andrienko, S. Shoaee, D. Neher, Barrierless free charge generation in the high-performance PM6:Y6 bulk heterojunction non-fullerene solar cell, Adv. Mater. 32 (2020) 1906763, https://doi.org/10.1002/adma.201906763.

[26] L.A.A. Pettersson, L.S. Roman, O. Inganäs, Modeling photocurrent action spectra of photovoltaic devices based on organic thin films, J. Appl. Phys. 86 (1999) 487–496, https://doi.org/10.1063/1.370757.

[27] G.F. Burkhard, E.T. Hoke, M.D. McGehee, Accounting for interference, scattering, and electrode absorption to make accurate internal quantum efficiency measurements in organic and other thin solar cells, Adv. Mater. 22 (2010) 3293–3297. http://10.0.5.91/journal.pmed.0020264.

[28] U. Rau, Reciprocity relation between photovoltaic quantum efficiency and electroluminescent emission of solar cells, Phys. Rev. B Condens. Matter 76 (2007) 1–8, https://doi.org/10.1103/PhysRevB.76.085303.

[29] C.-Y. Chan, Y.-C. Wong, M.-Y. Chan, S.-H. Cheung, S.-K. So, V.W.-W. Yam, Hole-Transporting spirothioxanthene derivatives as donor materials for efficient small-molecule-based organic photovoltaic devices, Chem. Mater. 26 (2014) 6585–6594, https://doi.org/10.1021/cm5033699.

[30] S. Zhang, L. Zuo, J. Chen, Z. Zhang, J. Mai, T.K. Lau, X. Lu, M. Shi, H. Chen, Improved photo-to-electron response of ternary blend organic solar cells with a low band gap polymer sensitizer and interfacial modification, J. Mater. Chem. A. 4 (2016) 1702–1707, https://doi.org/10.1039/c5ta09727d.

[31] K. Hussain, W. Kaiser, A. Gagliardi, Effect of polymer morphology on dilute donor organic solar cells, J. Phys. Chem. C 124 (2020) 3517–3528, https://doi.org/10.1021/acs.jpcc.9b11609.

[32] K. Vandewal, K. Tvingstedt, A. Gadisa, O. Inganäs, J. V Manca, Relating the open-circuit voltage to interface molecular properties of donor:acceptor bulk heterojunction solar cells, Phys. Rev. B 81 (2010) 125204, https://doi.org/10.1103/PhysRevB.81.125204.

[33] S. Ullbrich, J. Benduhn, X. Jia, V.C. Nikolis, K. Tvingstedt, F. Piersimoni, S. Roland, Y. Liu, J. Wu, A. Fischer, D. Neher, S. Reineke, D. Spoltore, K. Vandewal, Emissive and charge-generating donor–acceptor interfaces for organic optoelectronics with low voltage losses, Nat. Mater. 18 (2019) 459–464, https://doi.org/10.1038/s41563-019-0324-5.

[34] T. Saito, S. ichiro Natsuda, K. Imakita, Y. Tamai, H. Ohkita, Role of energy offset in nonradiative voltage loss in organic solar cells, Sol. RRL. 4 (2020) 2000255, https://doi.org/10.1002/solr.202000255.